Proceedings of ASME Turbo Expo 2014: Turbine Technical Conference and Exposition
GT2014
June 16 – 20, 2014, Düsseldorf, Germany

GT2014-26285

THREE-DIMENSIONAL VELOCITY MEASUREMENTS AROUND AND DOWNSTREAM OF A ROTATING VERTICAL AXIS WIND TURBINE

Kevin J. Ryan
Department of Mechanical Engineering
Stanford University
Stanford, CA 94305
Email: kjryan@stanford.edu

Filippo Coletti
Department of Mechanical Engineering
Stanford University
Stanford, CA 94305

John O. Dabiri
Graduate Aeronautical Laboratories and Bioengineering
California Institute of Technology
Pasadena, CA 91125

John K. Eaton
Department of Mechanical Engineering
Stanford University
Stanford, CA 94305

ABSTRACT

Modern designs for straight-bladed vertical axis wind turbines (VAWTs) feature smaller individual footprints than conventional horizontal axis wind turbines (HAWTs), allowing closer spacing of turbines and potentially greater power extraction for the same wind farm footprint. However, the wakes of upstream turbines could persist far enough to affect the performance of closely-spaced downstream turbines. In order to optimize the inter-turbine spacing and to investigate the potential for constructive aerodynamic interactions, the complex dynamics of VAWT wakes should be understood. The full three-component mean velocity field around and downstream of a scaled model of a rotating VAWT has been measured by Magnetic Resonance Velocimetry (MRV). The model turbine has an aspect ratio (height/diameter) of 1, and was operated in a water facility at subscale but still turbulent Reynolds number of 11,600 based on the turbine diameter. The main flow features including recirculation bubble sizes and strong vortex structures are believed to be representative of flow at full scale Reynolds number. To have kinematic similarity with a power-producing turbine, the model turbine was externally driven. Measurements were taken with the turbine stationary and while driven at tip speed ratios (TSRs) of 1.25 and 2.5, realistic values for VAWTs in operation. The MRV measurement produced three-dimensional velocity data with a resolution of 1/50 of the turbine diameter in all three directions. The flow is shown to be highly three dimensional and asymmetric for the entirety of the investigated region (up to 7 diameters downstream of the turbine). The higher TSR produced greater velocity defect and asymmetry in the near wake behind the turbine, but also showed faster wake recovery than the slower TSR and stationary cases. Wake recovery is affected by a counter-rotating vortex pair generated at the upwind-turning side of the turbine, which mixes faster fluid from the freestream in with the wake. The strength of vortices is shown to increase with TSR.

NOMENCLATURE

D	Turbine diameter
H	Turbine height
SNR	Signal-to-noise ratio
U	Velocity
δ_v	MRV experimental uncertainty
Ω	Turbine rotational frequency
λ	Tip speed ratio

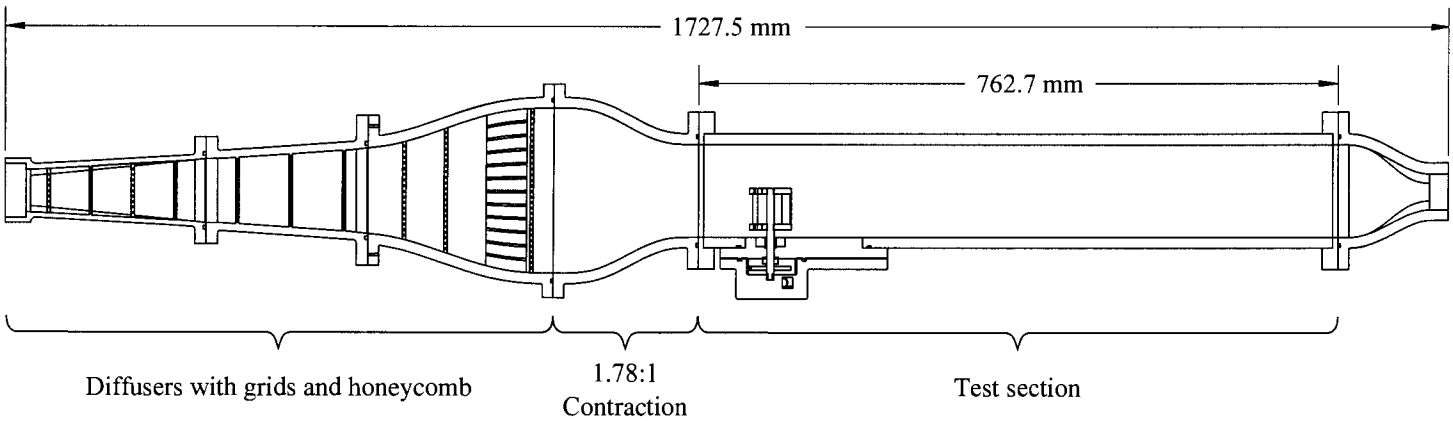

FIGURE 1: SCHEMATIC OF WATER TUNNEL

INTRODUCTION

A well-known limitation of renewable energy sources is that they are more diffuse than fossil fuels, and therefore large land surfaces are required to generate significant power. Wind energy is especially penalized, because conventional horizontal axis wind turbines (HAWTs) must be spaced far from each other (3-5 turbine diameters apart in the cross-wind direction and 6-10 diameters apart in the downwind direction [1, 2]) to avoid aerodynamic interference from their long and unsteady wakes. The choice of wind farm sites is further influenced by zoning acceptance restrictions, which often limit the installation of wind turbines to remote and sometimes offshore locations, away from populated areas that have higher energy demands.

Vertical-axis wind turbines (VAWTs) can be more closely spaced than conventional HAWTs, which points to a potentially greater power that can be extracted from a given wind farm footprint. Various observations support this view. First, the swept area of a VAWT can be increased independently of its footprint by increasing the rotor blade height. Second, recent studies show that the distance required to recover 95% of the upwind velocity behind a 10 m tall, 1.2 m diameter, straight-bladed VAWT is 4 turbine diameters, versus the 15 diameters needed for a HAWT [3]. Finally, it has been hypothesized that optimal layouts of VAWT arrays may benefit from constructive aerodynamic interactions between adjacent turbines [4]. Following these arguments, it has been recently proposed that the power density of a VAWT array may be an order of magnitude higher with respect to a conventional HAWT farm.

The above considerations on VAWTs are based on results obtained with velocity measurements of limited resolution, mostly confined to the vertical centerplane downstream of the turbine [5]. In fact, very few reports in the open literature describe the flow around VAWTs. Dixon et al. [6] investigated the detailed airfoil aerodynamics using two-dimensional PIV along a plane perpendicular to the turbine axis. Battisti et al. [7] focused on the wake characteristics along a plane normal to the flow, 1.5 turbine diameters downstream of the rotor axis. Ferreira et al. [8] looked at the shedding of tip vortices and their development in a VAWT wake both numerically and experimentally using PIV. Hofemann et al. [9] studied the effects of blade tip shape on the evolution of tip vorticies in the near wake region. Ferreira et al. [10] performed phase-locked hotwire measurements of streamwise velocity upstream, downstream, and at limited regions within a spinning VAWT. Because the flow field around the turbines is highly complex, there is the need for three-dimensional and volumetric velocity measurements.

High resolution, 3D, time-resolved simulations of the flow around VAWTs are still not available, and for calculations of large arrays they are expected to be prohibitively expensive in the foreseeable future. Past studies have assumed that the turbine has similar aerodynamics to a porous spinning cylinder [11]. Such simplified models need to be based on in-depth understanding of the fluid dynamics, and informed by reliable experimental data.

The full three-component mean velocity field has been measured around and downstream of a scaled-down model of a rotating VAWT by Magnetic Resonance Velocimetry (MRV, [12]). Two tip speed ratios (defined as the tangential blade velocity divided by the upwind flow speed) have been investigated and compared with a baseline case of the non-rotating turbine. Besides illustrating the wake dynamics, the results can inform low-order models and provide data for optimal wind farm design.

EXPERIMENTAL METHODOLOGY

Set-up and Flow Regimes

Measurements are carried out using water as a working fluid, with the addition of copper sulfate at 0.06 mol/L, in order to enhance the MRV signal. The water tunnel, sketched in Fig. 1, consists of several sections fabricated using stereolithography and assembled together in a channel 1730 mm in length. Three dif-

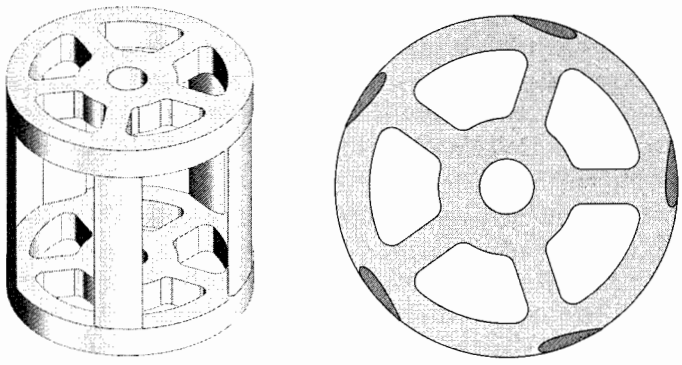

(a) 3D VIEW OF TURBINE

(b) CROSS-SECTION SHOWING AIRFOILS

FIGURE 2: VERTICAL AXIS WIND TURBINE MODEL WITH ASPECT RATIO 1

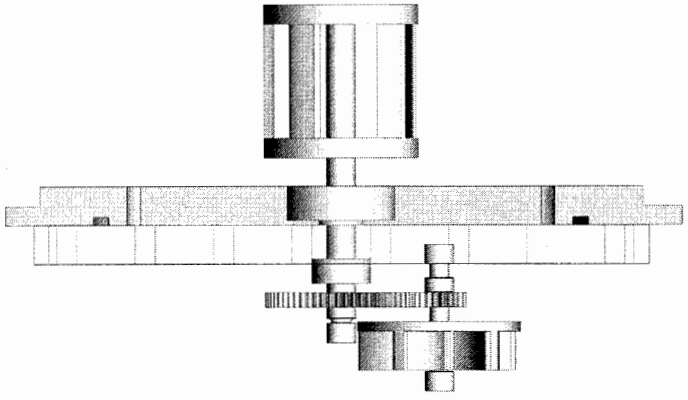

FIGURE 3: SCHEMATIC OF HYDRAULIC SPINNING MECHANISM WITH PADDLEWHEEL AND GEARING. GEAR RATIO IS CHANGED TO ACHIEVE DESIRED TSR.

fusers transform the circular inlet with a diameter of 38 mm to a square section of 196 mm by 196 mm. Nine grids in the diffusing sections prevent separation, and are followed by a honeycomb and a final grid to remove large scale secondary flows. A contraction of area ratio 1.78:1 connects to the 196 mm by 110 mm test section. The latter is 760 mm long, and its end is flanged to a piece that smoothly connects to the 38 mm outlet.

The turbine model is depicted in Fig. 2 and consists of 5 airfoils extruded between two 5-spoke disks, with a post running through the axis. NACA0018 airfoils are used with a maximum thickness of 1.8 mm, and the final 0.3 mm of chord length truncated for manufacturability, resulting in trailing edge thickness of 0.15 mm. Both the diameter D and the height H of the turbine model are 50 mm. The design of the model is influenced by 5 bladed VAWTs with aspect ratio of approximately 1 that are commercially available from WEPOWER. The results of the present

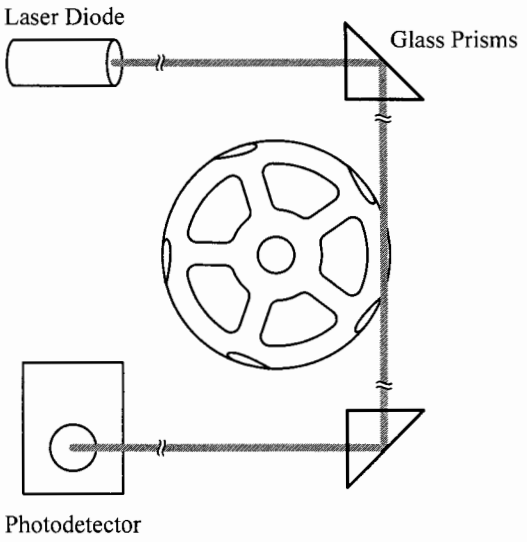

FIGURE 4: SCHEMATIC OF LASER TACHOMETRY SETUP SHOWING LASER LIGHT PATH THROUGH TURBINE. ROTATION OF TURBINE CAUSES AIRFOILS TO INTERRUPT LASER LIGHT, WHICH IS MEASURED BY PHOTODETECTOR.

study will complement future investigations on one such VAWT. The model is manufactured by stereolithography with less than 0.1 mm resolution, except for the post which is made of PVC and press-fitted into the turbine. The diameter of the post is 9.5 mm, which was chosen for rigidity. The post spins inside bearings embedded in the wall of the test section (Fig. 3).

At the relatively small scale of the present set-up, the torque exerted on the turbine by the water flow is not sufficient to overcome the friction in the seals and bearings. Therefore, the turbine is driven externally at the desired rotational speed. This implies that the experiment is in kinematic (rather than dynamic) similarity with an actual VAWT. Since the presence of metal near the region of interest would lead to artifacts in the MRV, driving the turbine with an electric motor is not a practical solution. Instead, a custom designed hydraulic spinning system is employed. A secondary water circuit drives a paddlewheel, enclosed in a chassis attached to the test section immediately below the turbine (Fig. 3). The paddlewheel transmits the motion to the turbine through a gearing system. The flow rate through the chassis is adjusted to provide the desired rotational speed of the turbine. The latter is measured using laser tachometry by shooting a light beam across the spinning turbine with a Thorlabs CPS180 laser diode, and capturing the chopped intensity via a Thorlabs DET36A photodetector. Figure 4 illustrates the measurement set-up. A real-time Fourier analysis of the photodetector signal provides the blade passing frequency, hence the turbine rotational speed.

The closed-loop flow system includes a holding tank, from

TABLE 1: GEOMETRICAL AND FLOW PARAMETERS

Parameter	Value
D [mm]	50
H [mm]	50
D_H [mm]	141
U_0 [m/s]	0.21
Re_{bulk}	32,700
Re_D	11,600
λ	0, 1.25, 2.5

which electric pumps extract the main flow and the secondary flow driving the turbine, which then recirculate back to the tank. The elements are connected by plastic hoses, 38 mm and 25 mm in diameter for the main and the secondary flow, respectively. The main flow is driven by two Berkeley BPDH10-L electric pumps, and the volume flow rate is measured by a Signet Instruments 8550 Flow Transmitter connected to a 515 Paddlewheel Flow Sensor. The secondary flow is driven by a Little Giant TE-6-MD-HC pump. The flow rate of the main flow is 270 l/min. The main flow Reynolds number, based on the channel hydraulic diameter D_H and the bulk velocity (U_0 = 0.21 m/s), is Re_{bulk} = 32,700, whereas the Reynolds number based on the turbine diameter is Re_D = 11,600. The tip speed ratio λ is defined in the equation:

$$\Omega D/2 = \lambda U_0 \tag{1}$$

where Ω is the rotational frequency. Three cases are considered and compared: λ = 0, 1.25, and 2.5. These tip speed ratios are chosen to reflect the range typically seen in operating turbines and investigated in other studies. The full scale VAWTs studied by Kinzel et al. [5] operate at a nominal tip speed ratio of 2.3. Battisti et al. measured wake profiles behind VAWTs with λ = 1.6 and $\lambda = 2.5$. Simulations performed by Castelli et al. [13] on a 5 bladed VAWT investigated the change in power coefficient, C_P, with tip speed ratio over λ = 1.44 to $\lambda = 3.3$ and found a peak in C_P at $\lambda = 2.0$. The main geometrical and flow parameters of the study are summarized in Tab. 1.

Experimental Limitations

The present study investigates a simplified model of realistic wind turbine conditions. The Reynolds number of the present study is high enough to create a turbulent wake behind the model turbine, but is 10 to 100 times smaller than Reynolds numbers for operational VAWTs, which typically run at Reynolds numbers of 10^5 to 10^6. While this precludes a direct comparison of the results of the present study with measurements of full-scale turbines, the fully turbulent wake suggests that the reported trends are expected to apply, at least qualitatively, at higher Reynolds number flow regimes.

The inlet flow conditioning includes a series of diffusers, grids, and a contraction that reduce the freestream turbulence in the test section. Although the MRV measurement technique does not provide a quantitative measurement of the turbulence in the test section, studies performed on other test sections with similar inlet flow conditioning show low levels of freestream turbulence. The resulting turbulence levels are below those a VAWT would experience while operating in atmospheric conditions. Low levels of turbulence in the turbine wake will reduce the amount of mixing of the wake with the faster freestream, increasing the wake recovery distance.

As previously mentioned, the turbine model is externally driven by a paddlewheel spinning mechanism. Since energy is being added to the flow by the external drive system, the results of the present study cannot be used in a turbine performance analysis from an energetic standpoint. The turbine is in kinematic similarity, therefore the flow structures that form around the turbine model are expected to be independent of the energy added or extracted by the turbine. Further downstream, the development of the wake is independent of the way the wake structures are formed. State-of-the-art methods for modeling wakes of VAWTs via CFD use a method equivalent to a driven turbine. Turbine blades are modeled as actuator lines and are moved through the CFD domain with one-way coupling to the fluid, without the fluid dynamics influencing the blade movement. The use of a driven turbine is justified by the best practices currently in use by the CFD wind energy community.

The restricted geometry of the test section causes the turbine model to create a significant blockage in the channel. The blockage ratio of the turbine is 12% based on the turbine frontal area, or 8.4% considering turbine solidity. Similar studies have blockage ratios of 10% to 25%, based on turbine frontal area. The blockage creates a *vena contracta* around the turbine, accelerating the flow in the freestream above that which would occur for a turbine operating in the open atmosphere. A large part of the blockage comes from the support structures of the airfoils, the center post and end disks, which could not be scaled to the same degree as the rest of the model, and are therefore larger than they would be in a full-scale turbine. The effect of these structures will be discussed in the results section on the 3D wake. The limited height of the test section also requires that the turbine model be located closer to the bottom wall than would occur in a VAWT in an operational installation. The proximity of the bottom wall and its effect on the wake development will be addressed in the results section.

Magnetic Resonance Velocimetry

Velocity data are obtained using the method of Magnetic Resonance Velocimetry (MRV) described by Elkins et al. [12]. MRV makes use of a technique similar to that used in medical Magnetic Resonance Imaging (MRI). Quantitative assessment of the three-component flow velocity is obtained due to the sensitivity of the phase of the MRI signal to motion. The procedure for the data acquisition technique is described by Pelc et al. [14]. The length of the acquisition process varies from 7 to 10 minutes for different TSR, and the acquisition is not phase-locked to the turbine rotation. Therefore the velocity fields acquired are time-averaged over the acquisition period. Six to eight acquisitions are performed for each region of interest and then averaged. Experiments are performed at the Richard M. Lucas Center for Imaging at Stanford University. A 3 Tesla General Electric whole body scanner is utilized. Three-component velocity measurements are obtained on a uniform Cartesian grid at a resolution of 1 mm in all three directions. The scanned volume includes both the flow and the solid walls of the test section. The wall identification is performed using a simple thresholding based on the signal magnitude: voxels with signal magnitude smaller than 10 times the magnitude of the average noise are identified as solid material. Changing the value of the threshold by $\pm 20\%$ produces no appreciable difference in the identification of the solid walls. For each investigated case a complete region of interest spanning the entire duct cross-section and extending from $-1.4D$ upstream to $6.9D$ downstream of the turbine axis is considered. Each data set is the combination of two regions of interest (235 mm by 110 mm by 196 mm each), slightly overlapping in the streamwise direction. Excluding the overlap, the data set for each tip speed ratio includes about 8.9 million data points. Acquisition and reconstruction for one data set takes roughly 5.5 hours.

Experimental Uncertainty

In MRV, the velocity encoding (*Venc*) values control the maximum measurable velocity that is free of aliasing. The expected uncertainty in the MRV measurements can be calculated from the formula (Pelc et al. [14]):

$$\delta_v = \frac{\sqrt{2}}{\pi} \frac{Venc}{SNR} \tag{2}$$

where the signal-to-noise ratio *SNR* is given by the ratio of the signal in the flow region over the signal in the solid wall. Different values of the velocity encoding were used for the upstream and downstream regions of interest. For the upstream and downstream sections, the uncertainties in the velocity when normalized by the bulk velocity are 6.2% and 4.3%, respectively. This includes both velocity measurement uncertainty as well as the effect of uncertainty in the precise location of the boundaries. The main flow rate was continuously monitored during the measurements. Fluctuations of the flow meter reading and small nonlinearities of its calibration result in an estimated uncertainty in the Reynolds number below 2%. The rotational speed of the turbine was also continuously monitored and recorded. The signal from the photodetector was acquired for 4 seconds at 400 Hz. A Fast Fourier Transform (FFT) was performed on the acquired signal, and the peak frequency for each 4 second interval was found over the length of the 7 to 10 minute long acquisition. The mean and variance of the peak frequencies gathered over multiple acquisitions were used to calculate mean rotational frequency and its uncertainty. The uncertainty in the measurement of the rotational frequency is about 4.8%. The variance of the rotational frequency and possible errors in the main flow measurement contribute to an uncertainty of about 5.1% on the tip speed ratio (at 95% confidence level).

RESULTS

This section presents selected data from the mean velocity fields obtained for the three cases, TSR = 0, 1.25, and 2.5. The results are normalized by the turbine diameter D and the bulk velocity U_0. X, Y, and Z indicate streamwise, wall-normal, and spanwise direction, respectively. The turbine rotates clockwise for an observer located at a higher Y position and looking down onto it. The turbine is represented in the same angular position in each plot. This is the actual position imposed during the stationary measurements.

Turbine Symmetry Plane

Figure 5 shows streamwise velocity contours along the XY symmetry plane of the turbine. The presence of the turbine produces significant blockage, and directs part of the incoming flow around the turbine. Because of the limited channel height, the flow accelerates in a *vena contracta* above the turbine. At TSR = 0 (Fig. 5a) the wake behind the turbine and the high velocity region above persist for the entire length of the measurement region. The extent of the wake decreases for increasing TSR, and indeed at TSR = 2.5 (Fig. 5c) the velocity distribution along the symmetry plane at the end of the measurement domain shows little sign of the presence of the turbine upstream. These observations are supported by profiles of streamwise velocity displayed in Fig. 6, which are extracted at the intersection of the turbine symmetry plane and a wall-parallel plane at the turbine mid height. The profiles indicate quicker wake recovery with increasing TSR, with the normalized streamwise velocity U/U_0 reaching 0.95 at $X/D = 5.5$ for TSR = 0, $X/D = 4.0$ for TSR = 1.25, and $X/D = 2.1$ for TSR = 2.5. The results of the wake recovery are seen in the the velocity profiles of streamwise velocity displayed in Fig. 7, which are extracted at $X/D = 6.5$ along the symmetry plane. The increasing uniformity of the velocity

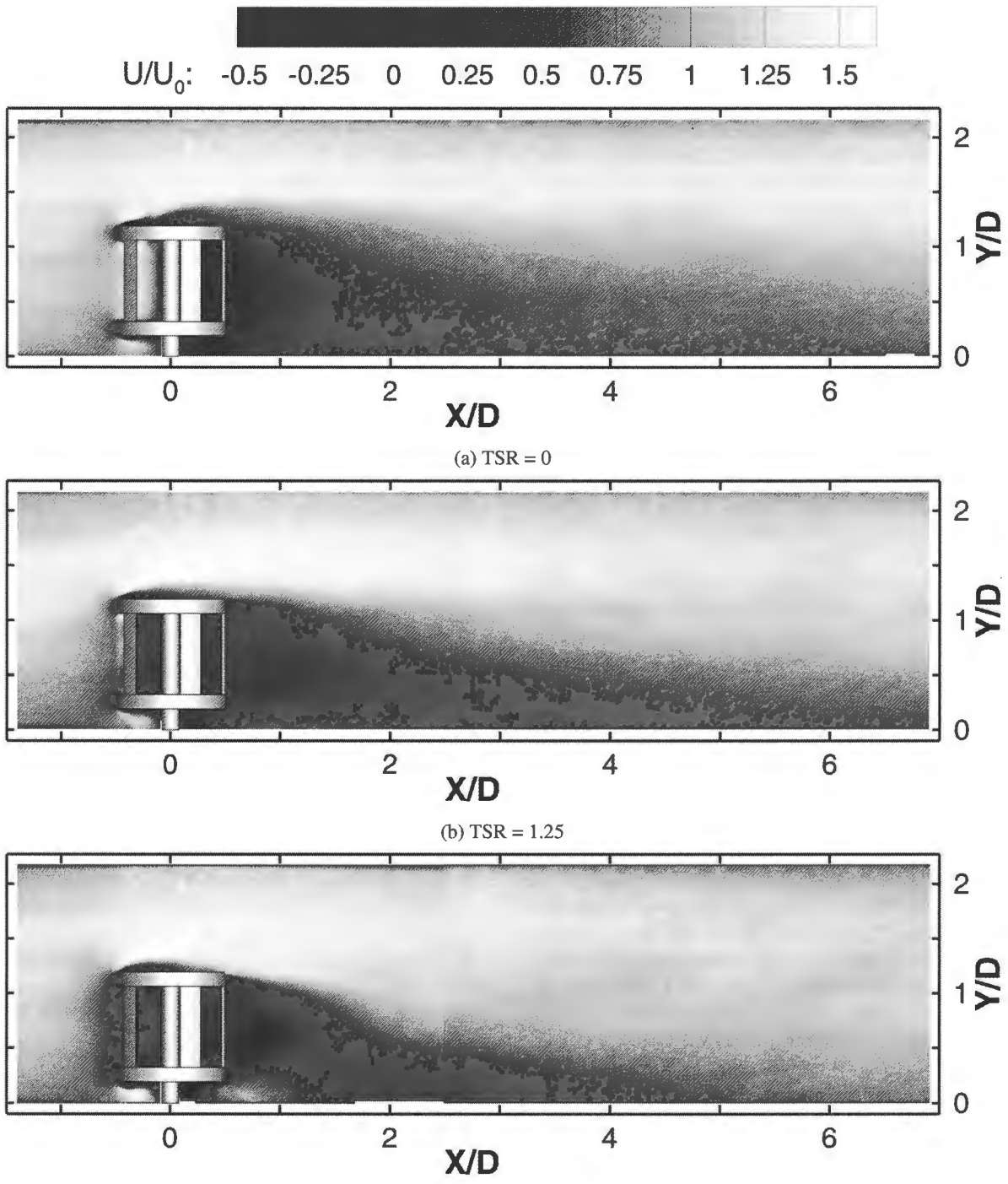

(a) TSR = 0

(b) TSR = 1.25

(c) TSR = 2.5

FIGURE 5: CONTOURS OF NORMALIZED STREAMWISE VELOCITY ALONG TURBINE SYMMETRY PLANE ($Z/D = 0$) SHOWING WAKE RECOVERY. STREAMWISE EXTENT OF DATA IS $X/D = -1.4$ TO $X/D = 6.9$.

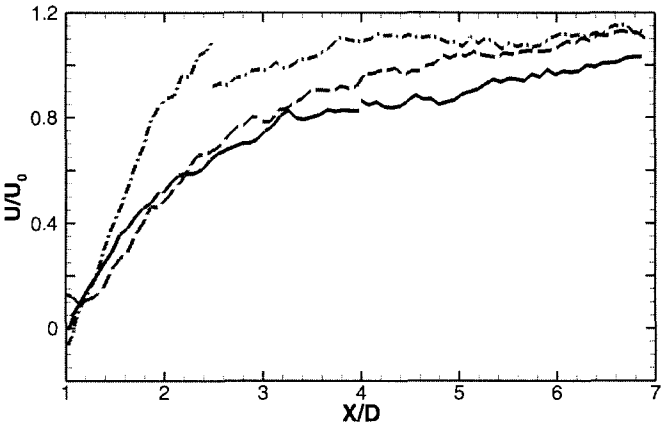

FIGURE 6: PROFILES OF STREAMWISE VELOCITY AS A FUNCTION OF STREAMWISE POSITION ALONG LINE THROUGH CENTER OF TURBINE ($Y/D = 0.7, Z/D = 0$) (— TSR = 0, – – – TSR = 1.25, – · – TSR = 2.5)

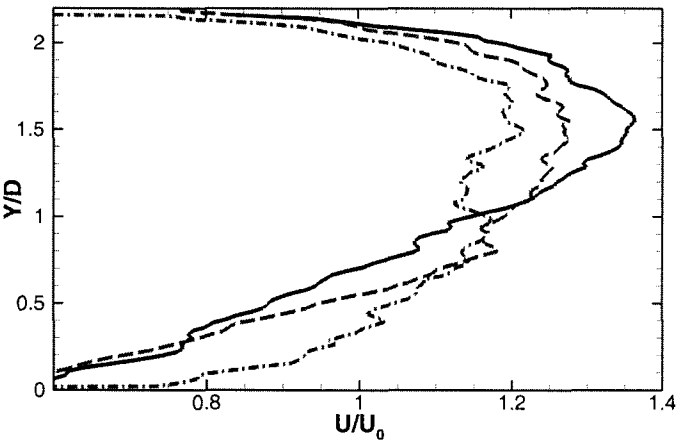

FIGURE 7: VERTICAL PROFILES OF STREAMWISE VELOCITY ALONG TURBINE SYMMETRY PLANE ($Z/D = 0$) AT $X/D = 6.5$ (— TSR = 0, – – – TSR = 1.25, – · – TSR = 2.5)

profiles are the result of quicker wake recovery with increasing TSR.

Axial Slices

Figure 8 shows cross-sections perpendicular to the main flow direction, colored by contours of streamwise velocity with overlaid vectors of in-plane velocity. Two streamwise locations, $X/D = 0$ and $X/D = 1.3$, are depicted for each TSR. For TSR = 0, the wake at $X/D = 1.3$ is approximately symmetric about the symmetry plane, and is largely contained in the area projected by the turbine. With increasing TSR the wake becomes wider and more asymmetric. The rotation of the turbine induces two counter-rotating vortices, originating from the side of the turbine that moves against the incoming flow. The vortices, which are stronger for higher TSR, entrain fluid from the high velocity regions above and on the opposite side of the turbine. By injecting high momentum fluid in the wake region, this mechanism causes the wake to recover faster, as indicated in Fig. 6. The strength of the counter-rotating vortex pair is likely reduced due to the presence of the end disks supporting the turbine blades. In turbine designs without end disks, the tip vortices shed by the blades would be stronger, mixing more freestream fluid with the wake and quickening wake recovery.

The effect of the bottom wall of the test section on the wake development can be seen in Figures 5 and 8. The proximity of the turbine to the bottom wall causes the turbine wake to interact with the boundary layer. The strength and cohesiveness of the bottom vortex of the vortex pair are reduced due to the presence of the wall, as shown in the velocity vectors in Figures 8b, 8d, and 8f. Additionally, the presence of the bottom wall keeps the streamwise velocity of the fluid below the turbine lower than the accelerated fluid above the turbine. Therefore not only is the bottom vortex of the pair weaker, but it is also only able to mix slow velocity fluid in the boundary layer with the fluid in the wake. The top vortex is able to mix higher velocity fluid into the wake, as is seen at the top of the wake in Figures 8d and 8f. This amounts to a top-bottom asymmetry in the wake recovery, evident in Figure 5.

3D Wake

The location and extent of the reverse flow region in the vicinity of the turbine is of particular importance in field measurements behind VAWTs, where single-point, single-component probes are often used. Such probes typically cannot discern between forward and reversed flow. Fig. 9 shows 3D isosurfaces at $U/U_0 = 0$, that enclose the volume of reverse flow around and behind the turbine for each case. Both lateral and top views are shown. The volume of the reverse flow region increases with tip speed ratio. For the stationary turbine (Fig. 9a,9b), the reverse flow regions are mainly due to the wakes behind the individual airfoils on the turbine and the post the turbine is mounted on. For the rotating turbine, the reverse flow behind the airfoils and post are no longer visible, and a reverse flow region caused by the movement of the turbine against the incoming flow develops. There exists a small recirculation region downstream of the post (not visible in Fig. 9), that is larger than would occur for a full-scale turbine, due to the relatively large size of the post used in the present study. At TSR = 1.25 (Fig. 9c,9d) the reverse flow region is found behind the turbine side moving against the main flow. The airfoils are moving only 25% faster than the incoming flow, therefore only a small volume of fluid is propelled upstream. At TSR = 2.5 (Fig. 9e,9f) the higher velocity of the airfoils produces a reverse flow that spans the en-

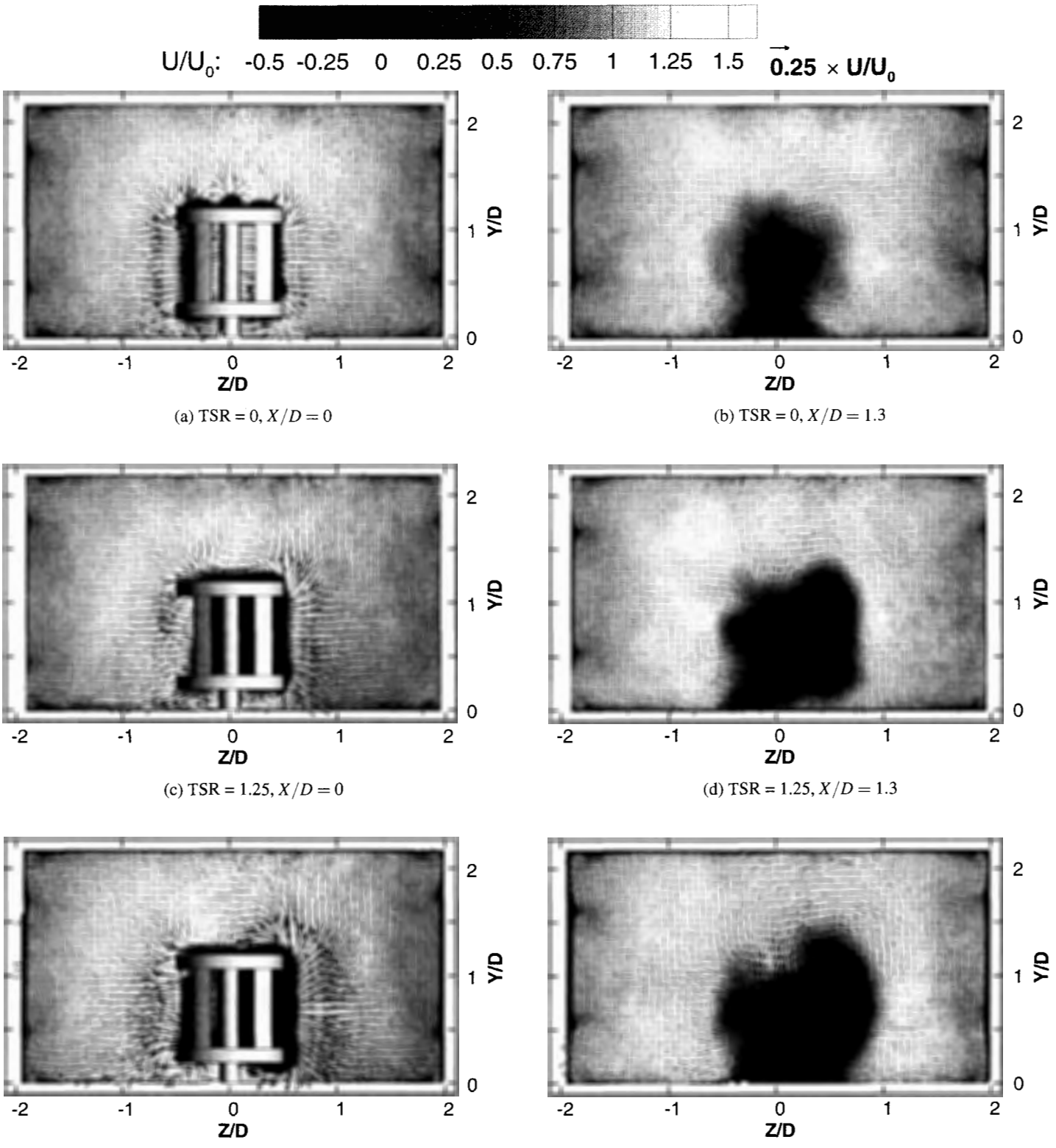

(a) TSR = 0, $X/D = 0$

(b) TSR = 0, $X/D = 1.3$

(c) TSR = 1.25, $X/D = 0$

(d) TSR = 1.25, $X/D = 1.3$

(e) TSR = 2.5, $X/D = 0$

(f) TSR = 2.5, $X/D = 1.3$

FIGURE 8: CONTOURS OF NORMALIZED STREAMWISE VELOCITY ALONG AXIAL PLANES $X/D = 0$ AND $X/D = 1.3$

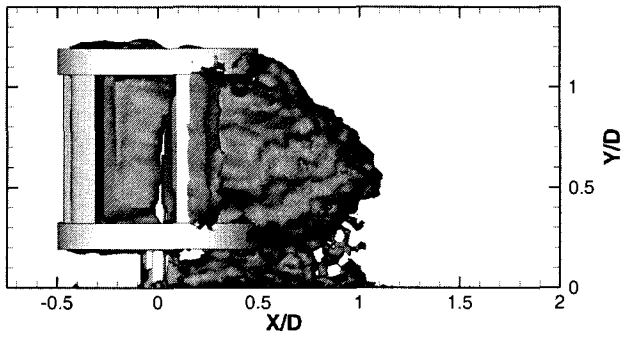

(a) TSR = 0, LATERAL VIEW

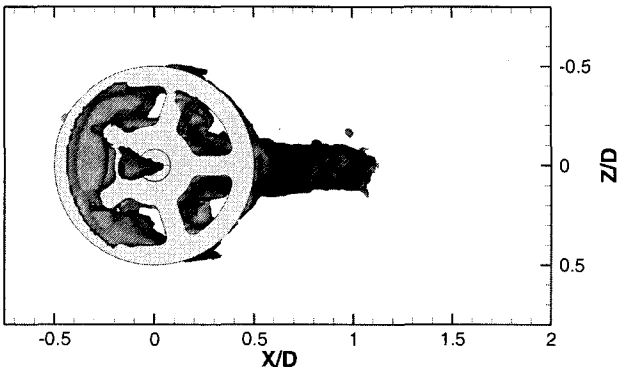

(b) TSR = 0, TOP VIEW

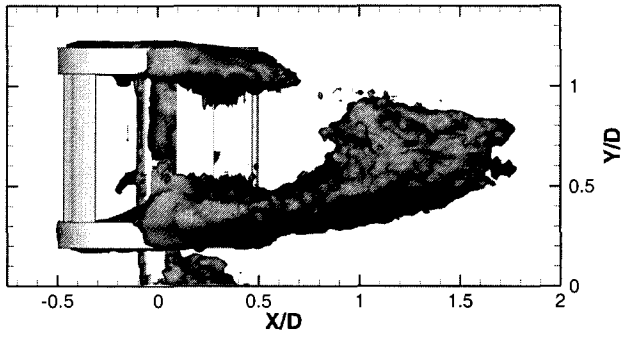

(c) TSR = 1.25, LATERAL VIEW

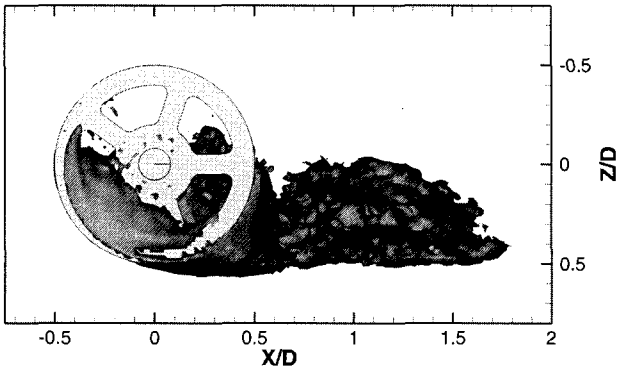

(d) TSR = 1.25, TOP VIEW

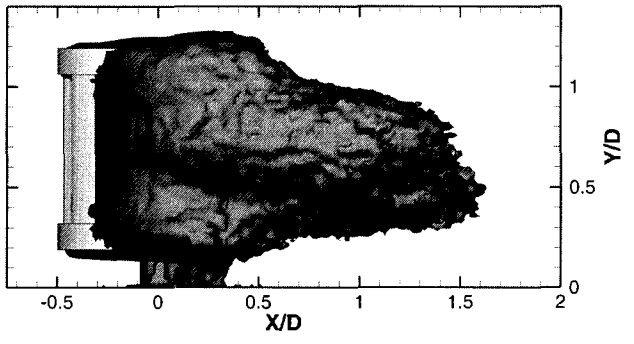

(e) TSR = 2.5, LATERAL VIEW

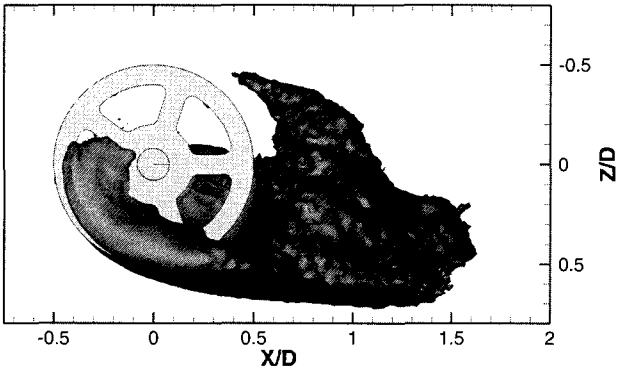

(f) TSR = 2.5, TOP VIEW

FIGURE 9: 3D ISOSURFACES OF $U/U_0 = 0$ IN NEAR WAKE OF TURBINE. VOLUME ENCLOSED BY ISOSURFACE INCREASES WITH TSR.

tire upwind-moving side of the turbine. Moreover, a reverse flow area exists on the opposite side of the turbine. This is because the high TSR causes significant tangential flow velocity along the downwind-moving side, resulting in high spanwise velocity component (see Fig. 8), which directs the flow laterally around the turbine rather than through it. The effect of the end disks can be seen in the lateral views of the 3D isosurfaces (Figs. 9c, 9e). At TSR = 1.25, the reverse flow region for $0 < X/D < 0.5$ is located by the end disks at the top and bottom of the turbine. The fluid near the end disks is always in contact with a moving solid surface, as opposed to the middle of the turbine, where the solid blades are only present 32% of the time. At TSR = 2.5,

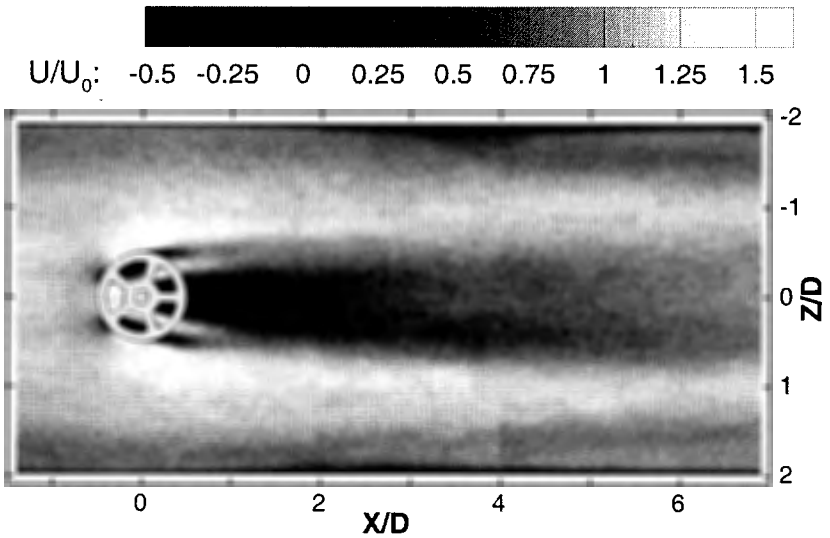

(a) TSR = 0

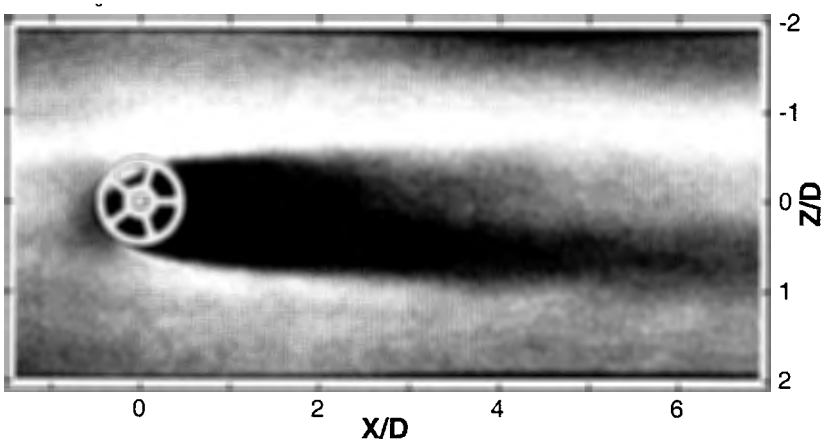

(b) TSR = 1.25

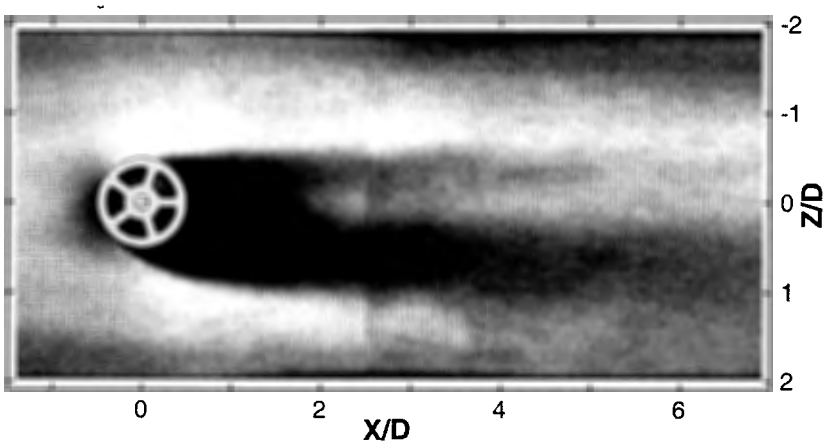

(c) TSR = 2.5

FIGURE 10: CONTOURS OF NORMALIZED STREAMWISE VELOCITY ALONG WALL-PARALLEL PLANE AT TURBINE MID HEIGHT ($Y/D = 0.7$)

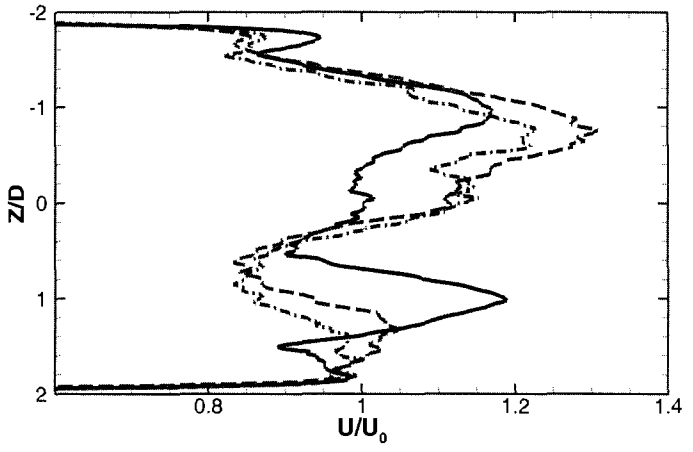

FIGURE 11: HORIZONTAL PROFILES OF STREAMWISE VELOCITY ALONG TURBINE MID HEIGHT ($Y/D = 0.7$) AT $X/D = 6.5$ (— TSR = 0, – – – TSR = 1.25, – · – TSR = 2.5)

the reverse flow region extends over the full height of the turbine (Fig. 9e). The movement of the blades alone is enough to cause reverse flow in the middle of the turbine, without the influence of the end disks.

Wall-Parallel Plane

Figure 10 shows contours of streamwise velocity along the wall-parallel plane at the mid height of the turbine ($Y/D = 0.7$). The near wake of the stationary turbine is the combination of the individual wakes of the turbine airfoils and the center post, and is approximately symmetric about the turbine symmetry plane. The rotation of the turbine in the rotating turbine cases causes a larger, connected wake region behind the turbine that persists up to about $X/D = 2$. In this region, the higher the TSR, the larger the asymmetry and the velocity defect of the wake. However, for approximately $X/D > 2$, the entrainment of faster fluid by the counter-rotating vortices (shown in Fig. 10) causes a faster recovery in the wake at TSR = 2.5 than at TSR = 1.25, and by the downstream end of the measurement domain the former case shows less asymmetry than the latter. The present experiments do not characterize the turbulence intensity, but it is likely that the higher TSR would be associated to a more turbulent wake, which enhances the momentum mixing and contributes to smear out the velocity defect. Figure 11 substantiates the discussion above, presenting profiles of streamwise velocity extracted at $X/D = 6.5$ along the plane at $Y/D = 0.7$. The profile of the stationary turbine is nearly symmetric, while the profiles behind the rotating turbine show, at this station, a somewhat more asymmetric wake at TSR = 1.25 than at TSR = 2.5.

CONCLUSIONS

The three-dimensional mean flow field around and downstream of a VAWT was measured at tip speed ratios between zero and 2.5. In order to provide indications for the layout and spacing of dense turbine arrays, the focus of this work was on the structure and extent of the wake. For the higher TSR, in the vicinity of the turbine (up to two turbine diameters from its axis) the wake is more asymmetric and displays stronger velocity defect. A large reverse flow region forms in the near wake, extending on both sides of the turbine axis. However, further downstream the wake recovers more quickly for higher TSR. This is due to a pair of counter-rotating vortices, generated on the slower side of the wake, which entrain high momentum fluid. The vortex strength, and therefore the wake recovery, is enhanced with increasing tip speed ratio. Indeed the flow along the vertical symmetry plane clearly shows a quicker wake recovery behind the rotating turbine compared to the non rotating one, and more so at higher TSR. It is concluded that, if one limits the analysis to the mean flow, higher TSRs are beneficial for the sake of minimizing aerodynamic interference between VAWTs by reducing the extent of an individual turbine's wake. The present analysis is strictly valid only for the specific turbine geometry studied. Further research is warranted that explores, for example, the effect of the aspect ratio. In general, the present study indicates that the three-dimensional description of the flow is critical for characterizing the wake of a VAWT.

The design of space-efficient wind farms of vertical axis wind turbines will require the use of accurate computational models. State-of-the-art models of VAWTs use the actuator line method to simulate turbine blades rotating in a flow field, but at present, there is an absence of high-resolution, three-dimensional, three-component velocity measurements needed to evaluate such models. The present study provides data against which models such as the actuator line model can be validated. The three-dimensional nature of the turbine wake exposed by the present study calls into question numerical simulations of the wake performed in 2D. Although such simulations would not be able to capture the full wake behavior a priori, they may be necessary to reduce the cost of the simulation of an entire wind farm. As such, the results of the present study can be used to improve 2D models of the wake development, to be applied at the middle of the turbine away from the ends. To be further applicable to the optimization of VAWT arrays in a wind farm arrangement, future work will focus on the interaction of wakes of two turbines.

REFERENCES

[1] Sørensen, B., 2004. *Renewable Energy: Its physics, engineering, environmental impacts, economics & planning.* Elsevier, London.

[2] Hau, E., 2005. *Wind Turbines: Fundamentals, Technologies, Application, Economics.* Springer, Berlin.

[3] Dabiri, J., 2011. "Potential order-of-magnitude enhancement of wind farm power density via counter-rotating vertical-axis wind turbine arrays". *Journal of Renewable and Sustainable Energy,* ***3***(4).

[4] Whittlesey, R., Liska, S., and Dabiri, J., 2010. "Fish schooling as a basis for vertical axis wind turbine farm design". *Bioinspiration & Biomimetics,* ***5***(3), p. 035005.

[5] Kinzel, M., Mulligan, Q., and Dabiri, J., 2012. "Energy exchange in an array of vertical-axis wind turbines". *Journal of Turbulence,* ***13***(38).

[6] Dixon, K., Simão Ferreira, C., Hofemann, C., van Bussel, G., and van Kuik, G., 2008. "A 3d unsteady panel method for vertical axis wind turbines". In The proceedings of the European Wind Energy Conference & Exhibition Brussels.

[7] Battisti, L., Zanne, L., Dell'Anna, S., Dossena, V., Persico, G., and Paradiso, B., 2011. "Aerodynamic measurements on a vertical axis wind turbine in a large scale wind tunnel". *ASME Journal of Energy Resources Technology,* ***133***(3), pp. 031201–1 – 031201–9.

[8] Ferreira, C., Hofemann, C., Dixon, K., van Kuik, G., and van Bussel, G., 2010. *3-D Wake Dynamics of the VAWT: Experimental and Numerical Investigation.* American Institute of Aeronautics and Astronautics.

[9] Hofemann, C., Simão Ferreira, C., Dixon, K., van Bussel, G., van Kuik, G., and Scarano, F., 2008. "3d stereo piv study of tip vortex evolution on a vawt". In EWEC 2008-European Wind Energy Conference-Brussels.

[10] Ferreira, C., van Kuik, G., and van Bussel, G., 2006. *Wind tunnel hotwire measurements, flow visualization and thrust measurement of a VAWT in skew.* American Institute of Aeronautics and Astronautics.

[11] Rajagopalan, R., and Fanucci, J., 1985. "Finite difference model for vertical axis wind turbines". *Journal of Propulsion and Power,* ***1***(6), pp. 432–436.

[12] Elkins, C., Markl, M., Pelc, N., and Eaton, J., 2003. "4d magnetic resonance velocimetry for mean velocity measurements in complex turbulent flows". *Experiments in Fluids,* ***34***(4), April, pp. 494–503.

[13] Raciti Castelli, M., De Betta, S., and Benini, E., 2012. "Effect of blade number on a straight-bladed vertical-axis darreius wind turbine". *World Academy of Science, Engineering and Technology,* ***61***, pp. 305–311.

[14] Pelc, N., Sommer, F., Li, K., Brosnan, T., Herfkens, R., and Enzmann, D., 1994. "Quantitative magnetic resonance flow imaging". *Magnetic Resonance Quarterly,* ***10***(3), pp. 125–147.